PCCP

PAPER

View Article Online
View Journal | View Issue

Cite this: *Phys. Chem. Chem. Phys.*, 2015, **17**, 3409

Co(III) protoporphyrin IX chloride in solution: spin-state and metal coordination revealed from resonant inelastic X-ray scattering and electronic structure calculations†

Kaan Atak,[ab] Ronny Golnak,[ac] Jie Xiao,[a] Mika Pflüger,[ab] Tim Brandenburg,[ab] Bernd Winter[a] and Emad F. Aziz*[abd]

Received 16th October 2014,
Accepted 12th December 2014

DOI: 10.1039/c4cp04703f

www.rsc.org/pccp

The local electronic structure of the cobalt centre-ion of Co(III) protoporphyrin IX chloride dissolved in dimethyl sulfoxide (DMSO) liquid solution is studied by resonant inelastic X-ray scattering (RIXS) spectroscopy at the cobalt L-edge. The resulting cobalt 2p partial-fluorescence-yield (PFY) X-ray absorption (XA) spectrum, integrated from RIXS spectra, is simulated for various possible spin-states and coordination of the cobalt centre by using the newly developed density functional theory/restricted open shell single excitation configuration interaction (DFT/ROCIS) method. Comparison between experiment and calculation shows that the cobalt ion ($3d^6$ electronic configuration) adopts a low-spin state with all six 3d electrons paired, and the cobalt centre is either 5-coordinated by its natural ligands (one chloride ion and four nitrogen atoms), or 6-coordinated, when binding to an oxygen atom of a DMSO solvent molecule. Analysis of the measured RIXS spectra reveals weak 3d–3d electron correlation, and in addition a value of the local HOMO–LUMO gap at the Co sites is obtained.

Introduction

Metalloporphyrins (MP) are a large family of organic molecules with diverse functionality in biological processes.[1] When embedded in protein molecules, such as heme in hemoglobin, MPs serve as a functional group of the protein, conducting ligand exchange (with oxygen or carbon monoxide), or harvesting sun light for storage in the form of chemical energy.[2] Most of the chemical and biological functions are essentially governed by the metal ion located at the porphyrin molecular centre.

Heme, containing an Fe^{2+} ion in the molecular centre, is one of the most important MPs in biological systems, which makes heme an interesting target in porphyrin researches. The experimental studies, however, are hampered by the instability of the Fe^{2+} ion which may be easily oxidized. Although condensed-phase heme can be prepared *in situ* on metal substrates under ultra-high vacuum condition,[3,4] heme molecule in solution eventually oxidizes, forming hemin. From experimental feasibility point of view the substitution of Fe^{2+} by Co^{3+} would arguably be an alternative candidate to study since both ions have $3d^6$ electronic configuration.[5–7] Note that the metal-centre functionality mainly originates from the valence orbitals at the metal sites. Indeed, cobalt(III) protoporphyrin IX chloride (CoPPIX-Cl), depicted in Fig. 1, has a rather similar ligand structure as heme (also shown in the figure), except for the extra chloride attached to the cobalt ion. In the present study, CoPPIX-Cl is dissolved in dimethyl sulfoxide (DMSO), mimicking a liquid environment relevant for biological (aqueous) systems.

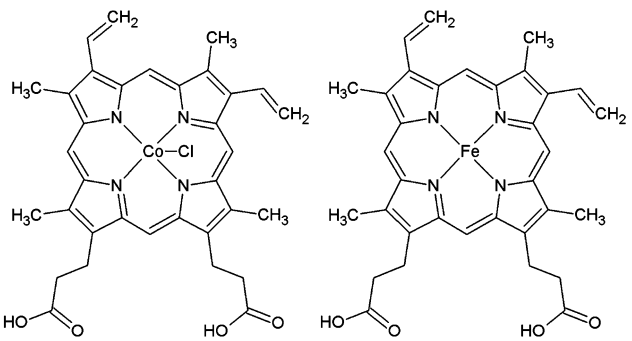

Fig. 1 Chemical structure representation of CoPPIX-Cl (left) and heme (right).

[a] *Institute of Methods for Material Development, Helmholtz-Zentrum Berlin für Materialien und Energie, Albert-Einstein-Strasse 15, 12489 Berlin, Germany. E-mail: emad.aziz@helmholtz-berlin.de*
[b] *Freie Universität Berlin, Fachbereich Physik, Arnimallee 14, D-14195 Berlin, Germany*
[c] *Freie Universität Berlin, Fachbereich Chemie, Takustr. 3, D-14195 Berlin, Germany*
[d] *Institute for Molecular Science, Myodaiji, Okazaki 444-8585, Japan*

† Electronic supplementary information (ESI) available: Geometric structure of the bond length/angle and the bond characters between Co centre and its ligand. See DOI: 10.1039/c4cp04703f

In order to probe the local electronic structure of the metal centre we have applied soft X-rays to resonantly excite cobalt 2p electrons into the partially occupied 3d levels. In tuning the photon energy across the full (L-edge) absorption band, we obtain a series of resonant X-ray emission spectra, also referred to as resonant inelastic X-ray scattering (RIXS) spectra.[8,9] Here, we specifically detect the strong, dipole allowed transitions from the various Co 3d-character states to the 2p core level (within an approximately 20 eV energy window). The intensity of a given spectrum reflects the relative X-ray absorption cross section. That is, signal integration of the RIXS spectra as a function of excitation photon energy delivers one possible partial-fluorescence-yield (PFY) XA spectrum, with a large sensitivity to valence electron delocalization, in the present case. As is also the case for other X-ray absorption measurements based on secondary processes (such as inverse fluorescence[10] or electron emission[11]) these partial-yield XA spectra as well as total-yield spectra (not considered though in this work) may however differ from the true absorption spectra obtained in a transmission measurement. Differences are due to the fact that certain fluorescence channels may compete with other non-radiative relaxation pathways, and hence the observed fluorescence is not exactly proportional to the number of absorbed photons.[12] We note though that these effects are likely to be minimized if one probes 2p core-level refills involving transitions from deeper (core) levels, *e.g.* 3s, because of too low signal intensities, owed to low solute concentration; these channels are not investigated here. In the present work we discuss the PFY-XA spectra with the help of a newly developed hybrid calculation method of density functional theory/restricted open-shell single excitation configuration interaction (DFT/ROCIS)[13,14] that simulates the XA spectra at the Co L-edge. Local coordination and spin-state character of the cobalt centre can be extracted by comparison of the experimental data with the theoretical calculations; this is analogous to our recent work on hemin.[15] The theoretical interpretation of the XA spectra is complemented by the rather qualitative analysis of the RIXS spectra which allows for an experimental identification of electronic decay channels, corresponding to the specific transitions from occupied and unoccupied orbitals to the cobalt 2p core levels. Experimental (relative) energies, including the local HOMO–LUMO gap, are discussed with respect to the calculated energies at the ground state.

Methods

Experiment

Co(III) protoporphyrin IX chloride (CoPPIX-Cl) with >98% purity was obtained from Frontier Scientific, and dimethyl sulfoxide (DMSO), >99% purity, was purchased from Sigma-Aldrich. A 50 mM solution was prepared by dissolving CoPPIX-Cl in DMSO. This solvent was chosen because higher CoPPIX-Cl concentrations can be achieved than in water which enhances the detected photon-signal intensity. In addition, porphyrin dimerization, which is common in aqueous solution, can be prevented.[16,17] RIXS (and the resulting XA) spectra at the Co L-edge were recorded using the LiXEdrom experimental station, equipped with a liquid-flow cell, at the U41-PGM undulator beamline of the Berlin synchrotron facility, BESSY II. Total acquisition time for the full $L_{3,2}$ edge XA spectrum was approximately 400 min, and includes measurement of 280 RIXS spectra in the 760–800 eV photon emission range (corresponding to 3d–2p transitions), for 775–803 eV excitation photon energy (at step width of 0.1 eV). In addition, several individual RIXS spectra were recorded at much increased collection time (40 min per spectrum) for improved signal-to-noise which allows identification of specific decay channels. A 100 nm thick Si_3N_4 membrane, which is part of the flow cell, separates the liquid solution from the vacuum inside the main experimental chamber. Details of the experimental setup have been described in our previous work.[18] Spectra were obtained using a Rowland-circle geometry spectrometer with a grating of 7.5 m radius and 1200 lines per mm, covering the soft X-ray energy range of 400–1000 eV. Because of the low CoPPIX-Cl concentration all measurements were performed with the grating angle set to the first diffraction order. For the present experiment energy resolution was set to approximately 0.5 eV, at 775 eV photon energy. The photon detector, which is operated at a pressure of approximately 10^{-8} mbar, consists of a MCP/phosphor screen-stack and a CCD camera.

Computation

The calculations were carried out with the ORCA program package.[19] Molecular geometry optimizations were performed using the B3LYP[20,21] density functional method with the def2-TZVP(-f) basis set.[22] Transition energies and moments for Co L-edge were calculated with DFT/ROCIS using the same basis set. For DFT/ROCIS calculations, the B3LYP functional together with the parameters $c_1 = 0.18$, $c_2 = 0.20$, and $c_3 = 0.40$ was applied.[14] These three universal parameters are to be distinguished from the empirical parameters in semi-empirical molecular-orbital theories. During the optimization calculations, the resolution of identity[23–27] approximation was used employing the def2-TZV/J auxiliary basis set.[28] Numerical integrations during the DFT calculations were performed on a dense grid (ORCA grid4). L-edge absorption spectra were obtained by applying a 1 eV Gaussian-type broadening on each transition moment, and then summing up. The geometry calculations had no symmetry constraint. Vibronic effects were not taken into account in the calculations.

Results and discussion

It is useful to first address the Co L-edge PFY-XA spectrum from the CoPPIX-Cl/DMSO solution, determine the energies of the most probable 2p–3d transitions, and explore the Co^{3+} ($3d^6$) spin multiplicity and possible ligand coordination. The experimental PFY-XA spectrum is presented in Fig. 2, top trace, and for comparison we also show six theoretical XA spectra accounting for various spin states and Co coordination. Since Co^{3+} has $3d^6$

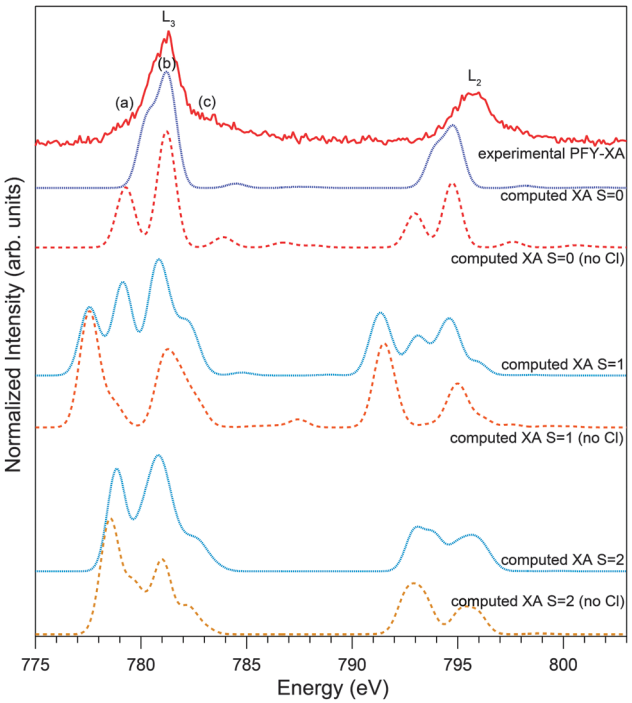

Fig. 2 Experimental cobalt L-edge PFY-XA spectrum (top red trace) from a solution of 50 mM CoPPIX-chloride dissolved in DMSO, along with the computed (using DFT/ROCIS) XA spectra for different spin multiplicities, in the presence and absence of chloride, respectively. Labels (a)–(c) refer to the photon absorption energies for which the RIXS spectra will be presented.

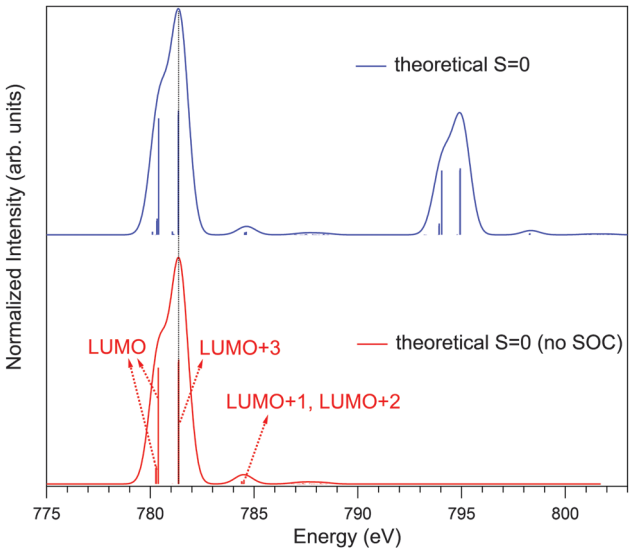

Fig. 3 Computed (using DFT/ROCIS) cobalt L-edge XA spectra for CoPPIX-Cl: S = 0 in the presence (blue trace) and in the absence (red trace) of spin–orbit coupling, respectively. Vertical sticks mark the calculated transition moments. The computed spectra are shifted *ad hoc* by 16.35 eV (blue trace) and 11.7 eV (red trace).

electron configuration, the spin multiplicity $2S + 1$ may adopt values 1, 3, 5, with S = 0, 1, 2, corresponding to an all-paired electron system ($S = 0$), a two-unpaired electron system ($S = 1$) and a four-unpaired electron system ($S = 2$), respectively. In addition, for each hypothetical spin state (the actual spin state is yet to be discussed) we also look at the effect of chloride being attached or not. This latter aspect is motivated by previous works on hemin in DMSO, reporting that chloride detaches from the Fe^{3+} centre[17,29] The respective geometric structures, shown in Fig. SI-1 of the ESI,† were first optimized by DFT calculations, and then transferred into the DFT/ROCIS routines to simulate XA spectra. It is seen from Fig. 2 that the spectrum for S = 0, and chloride attached (structure A of Fig. SI-1, ESI†), matches the experiment best. Another important observation from Fig. 2 is that the spectral shape is very sensitive to both spin state and Co–Cl coordination. The four simulated spectra for $S > 0$ tend to exhibit an overall richer structure, dispersed over a larger energy range. However, the simpler structure for the $S = 0$ case is in better agreement with experiment. Spin state has also a quite pronounced effect on the molecular structure; the effect of increasing spin state on the geometric structure of CoPPIX-Cl is a slight protrusion of Co above the molecular plane (Fig. SI-1, ESI,† top view). Numerical values of theses bond distances and also of the respective bond angles are presented in Table SI-1 of the ESI.†

In order to determine the molecular orbital (MO) contributions to the individual X-ray absorption transitions, we re-plot in Fig. 3 (upper trace) the best matching simulated spectrum from Fig. 2, *i.e.*, the blue trace for low-spin S = 0 state and 5-coordination, along with the respective calculated transition moments as vertical bars. We also present the calculated spectrum with spin–orbit-coupling (SOC) excluded with its individual transition moments, shown in the bottom of Fig. 3. In this latter case assignment of the transition moments to individual MOs is much facilitated as the number of transitions reduces from hundreds (SOC-included, upper trace) to dozens. Such a simplification still correctly describes the overall orbital character, and preserves almost all spectral features at the Co L_3 edge, as is also demonstrated in our previous work.[15] We also note that the simulated spectra along with their transition moments (vertical bars) were adjusted in energy in order to match the experimental spectrum. Furthermore, the spin–orbit splitting of the Co 2p level (L_3–L_2 energy difference) is underestimated by ~1 eV. These shortcomings are intrinsic to the DFT/ROCIS method[14] but insignificantly affect our interpretation; see also our previous discussion in ref. 15. Our analysis below will reveal the details of the absorption peak (Fig. 3, bottom), and we will construct a local electronic structure map around the cobalt ion.

Population analysis by DFT calculations for the 5-coordination structure, and S = 0, reveals both the atomic contributions from cobalt and its nearest neighbours to the MOs, as well as the percentage of different cobalt d-orbitals within the considered energy range. The results are presented as chart diagrams in Fig. 4a and b, respectively. In addition, we depict in Fig. 5 multiple valence orbitals (their spatial distributions and energies) that have considerable cobalt contributions, including the unoccupied MOs with significant contributions to the XA transitions. Other occupied orbitals will be addressed along with our discussion of the RIXS spectra, below. From the ground-state DFT calculation we thus infer that MO 170 is the lowest

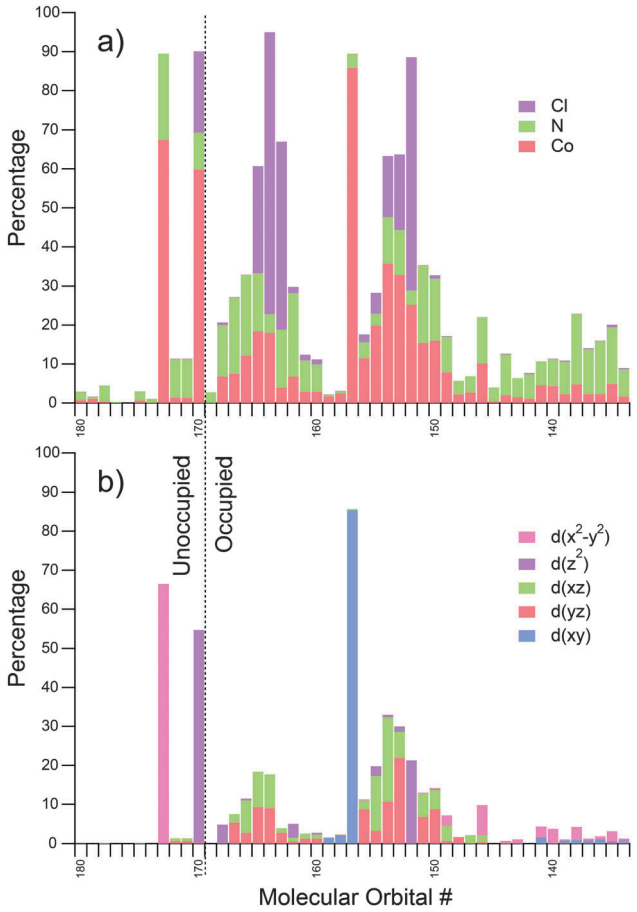

Fig. 4 The molecular orbital character obtained from single-point DFT calculations for CoPPIX-Cl. (a) Relative contributions of cobalt and its nearest neighbors. (b) Contributions from the different cobalt d-orbitals, obtained from restricted closed shell single point DFT calculation, using Löwdin population analysis.

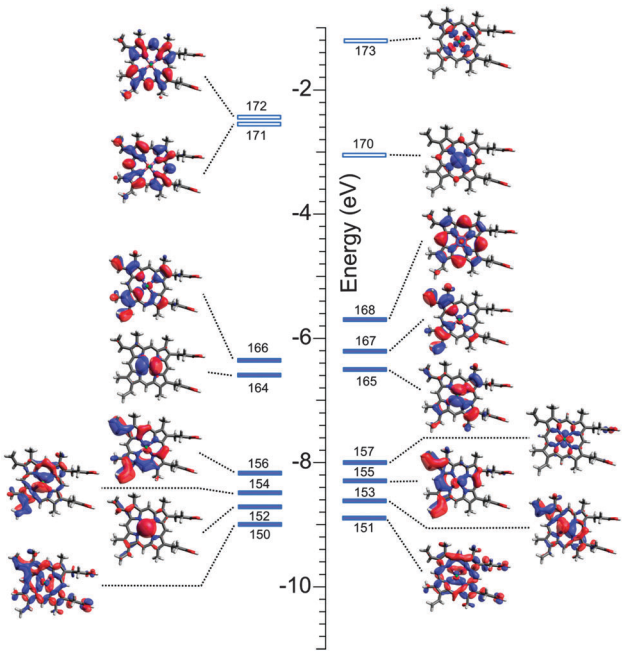

Fig. 5 Calculated valence orbitals (and their energies) with significant cobalt contributions for CoPPIX-Cl in the ground state for 5-coordination, and lowest-spin, $S = 0$, as obtained from the restricted closed shell single point DFT calculations.

unoccupied molecular orbital (LUMO), and the main contributions to the XA spectrum of Fig. 3 (bottom) are the 2p to LUMO and LUMO + 3 (MO 173) transitions. Together with Fig. 4b we find that these unoccupied orbitals are largely of d_{z^2} and $d_{x^2-y^2}$ character, resulting from the 3d energy splitting in an approximate square-pyramidal (C_{4v}) ligand-field symmetry. Having nodes between cobalt and its nearest neighbours, these orbitals are essentially anti-bonding. The small XA peak at higher photon energy, near 785.5 eV (Fig. 3, bottom), is identified as the 2p – LUMO + 1 (MO 171) and 2p – LUMO + 2 (MO 172) transitions. Both orbitals have mainly nitrogen character, and less of cobalt contributions (d_{xz} and d_{yz}), indicating that the respective transitions are metal-to-ligand charge transfer (MLCT) in nature. Notice that for the molecular ground-state LUMO + 1 and LUMO + 2 energies are in between the LUMO and LUMO + 3 energies, and yet higher photon energy is required (see Fig. 3, bottom) for their population by a cobalt 2p electron. This suggests an alteration of orbital energies due to the highly perturbed nature of core-hole-excited state. Considering the stronger nitrogen character of the LUMO + 1 and LUMO + 2, we argue that populating these orbitals by a cobalt core-level electron may require additional energy relative to LUMO + 3 that has mainly cobalt character. This leads to the observed change of the energetic ordering in the excited state.

It is instructive to compare the favourable low-spin case of CoPPIX-Cl in the 5-coordinated geometry with the findings for hemin. Dissolved in the same DMSO solvent, the $Fe^{3+}(3d^5)$ ion assumes a high-spin state in the 5-coordinated geometry but it has a tendency to acquire low-spin configuration in the 6-coordinated geometry.[30] Apparently, the analogous situation does not apply for Co^{3+} in CoPPIX-Cl that adopts low-spin state and 5-coordination structure as we discussed. This raises the question whether Co^{3+} can acquire a sixth ligand, say, from the solvent since it is already in the low-spin state. However, adding a sixth ligand is unlikely to change the spin state. In order to complete the spin-coordination argument, we also explored the 6-coordination configuration. For this we have computed the XA spectrum of CoPPIX-Cl in a structure where the cobalt centre binds to an additional oxygen atom, the oxygen site of the DMSO solvent. The resulting XA spectrum is depicted in Fig. SI-2 (ESI†), and the corresponding structure is shown in Fig. SI-3 (ESI†) ($S = 0$). The spectrum is indeed very similar to the one calculated for the respective 5-coordination geometry, and both are in good agreement with our experimental spectrum; all three spectra are presented in Fig. SI-2 (ESI†). Very likely both 5- and 6-coordinated geometries co-exist in solution but an experimental quantification of the relative amounts is not possible at the present moment.

Regarding experiment, we have so far only discussed the partial (3d–2p)-yield X-ray absorption spectrum which is obtained by integration of many individual RIXS spectra, and these are in

fact the actual spectra measured in the experiment. More importantly, the RIXS spectra contain information (which is lost in the XA spectrum due to the integration) on the states involved in the electronic de-excitation process, and this includes the occupied valence orbitals. As was pointed out earlier[15] the computation of L-edge RIXS spectra with ORCA is not yet implemented in the ORCA package, and we have to discuss our findings rather qualitatively, yet revealing significant new electronic-structure details. For our analysis we will consider few explicit RIXS spectra (mapping aforementioned 3d–2p transitions), which were each acquired for much longer time, approximately factor 24, than the individual RIXS spectra, measured at an excitation step width of 0.1 eV, giving rise to the XA spectrum of Fig. 2, in order to yield spectra with reasonably good signal-to-noise. We chose RIXS spectra measured at 781.3 eV and 795.7 eV excitation photon energies, corresponding to peak maxima in the respective cobalt L_3 and L_2 edge XA spectra (see Fig. 2, top), and we also select spectra measured at the respective absorption onset (pre-edge), and at a photon energy approximately 1.5 eV above the cobalt $2p_{1/2,3/2}$–3d resonance. Results are presented in Fig. 6; energies are shown as emitted photon energy rather than energy losses, and intensities are scaled to yield the same peak heights at maximum photon emission. In the following discussion we largely focus on the L_3-edge, *i.e.*, on the three bottom spectra of Fig. 6.

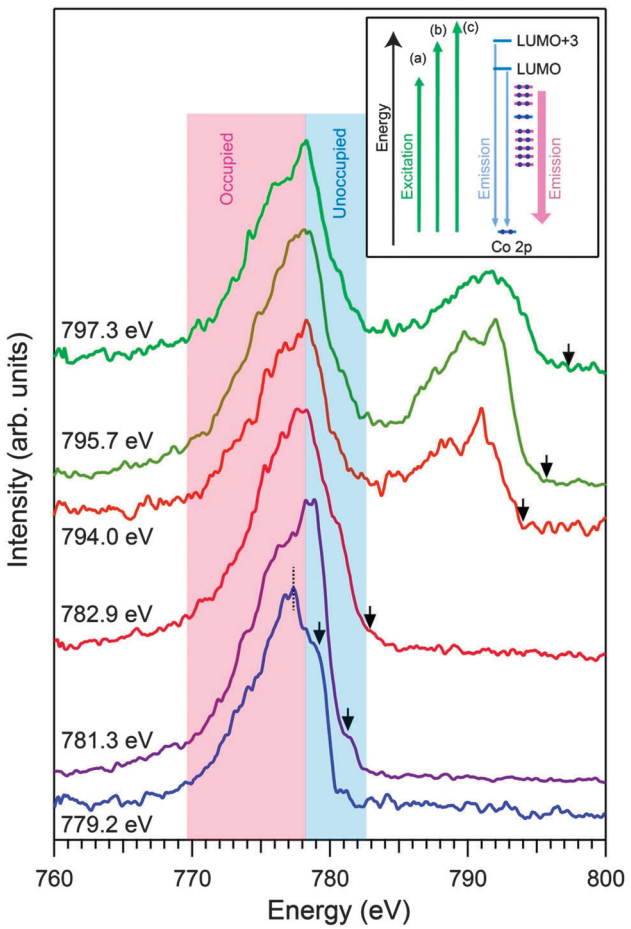

Fig. 6 Cobalt L-edge RIXS spectra from 50 mM CoPPIX-Cl in solution, measured at selected excitation energies; see text for details. The pink-shaded area indicates the doubly occupied molecular orbitals (DOMOs), and the blue-shaded area highlights the unoccupied orbitals. Black small arrows indicate the energies of the elastic peak. The inset is a schematic representation of the observed X-ray excitation and de-excitation transitions along with the relevant orbitals.

For all excitation photon energies the RIXS spectra are seen to be almost identical within the approximately 770–778 eV energy range. This emission range, pink-shaded in Fig. 6, is well below the onset (pre-edge, feature (a) in Fig. 2) of the experimental XA spectrum, and is thus attributed to transitions from doubly occupied molecular orbitals (DOMOs) into cobalt $2p_{3/2}$. The insensitivity to excitation energy is a clear implication of a weak 3d–3d electron correlation. To support our spectral assignment we consider the inset of Fig. 6 which is a schematic representation of the experimental excitation (2p–3d) and emission (3d–2p) energies, as well as of the calculated cobalt orbital energies. The depicted excitation energies (represented by green arrows in the inset) refer to the lowest-energy X-ray absorption ((a) from Fig. 2), which is somewhat below the $2p_{3/2} \rightarrow 3d_{z^2}$ (LUMO) transition, and maximum absorption (b) corresponds to the $2p_{3/2} \rightarrow 3d_{x^2-y^2}$ (LUMO + 3) transition. The approximately twice as large intensity for the $2p_{3/2} \rightarrow 3d_{x^2-y^2}$ transition as compared to the $2p_{3/2} \rightarrow 3d_{z^2}$ transition, observed in Fig. 3, reflects the difference in the respective density of states of the 2p core-level. Feature (c) corresponds to a post-edge absorption due to the MLCT transitions (LUMO + 1, LUMO + 2) that require higher energies than $3d_{x^2-y^2}$, as discussed above. For excitations (a) and (b) the corresponding elastic-scattering peaks are clearly visible in the spectra, and indicated by small arrows. With reference to the energy scheme in Fig. 6 (inset) we can now determine the local HOMO–LUMO gap from experiment. We begin with a closer inspection of the RIXS spectrum at the excitation energy 779.2 eV (a), Fig. 6, bottom. At this energy a Co $2p_{3/2}$ electron is excited into the LUMO, and the observed (elastic) peak, again shown by small black arrow, thus corresponds to the LUMO $\rightarrow$ $2p_{3/2}$ electron refill (blue arrow in inset figure). Emission at lower energies than the elastic peak is due to HOMO $\rightarrow$ $2p_{3/2}$ (pink arrow) and other lower-lying DOMO $\rightarrow$ $2p_{3/2}$ transitions. The approximately 1.8 eV energy difference between the elastic peak and the onset of the latter transitions (marked by a vertical dashed line) is thus the HOMO–LUMO gap at the Co site. This experimental value is not in a good agreement with the 2.6 eV difference between MO 170 (LUMO) and MO 168 (HOMO − 1) in Fig. 5. Note however that MO 169, which is the actual molecular HOMO, has no metal contribution, and is thus not probed in the present experiment. This energy mismatch mirrors the rather limited value of ground-state DFT calculation for the interpretation of core-hole excitation spectra. As we tune the excitation photon energy to the maximum L_3-edge absorption, at 781.3 eV (b), we observe in addition to the elastic peak, which is LUMO + 3 $\rightarrow$ $2p_{3/2}$, emission due to the LUMO $\rightarrow$ $2p_{3/2}$ transition. Since the LUMO is not directly populated by absorption of a 781.3 eV photon, its population is most likely by a shake-up process, involving promotion of an electron from occupied valence states. Shake-up processes occur also for all

higher excitation energies, particularly at the L_2-edge, in which case LUMO + 3, LUMO → $2p_{3/2}$ transitions are still being observed (giving rise to the signal in the blue-shaded energy region in Fig. 6). Here the electron promotion from occupied valence states to LUMO (shake up) is initiated by ionization of the Co $2p_{3/2}$ level. Alternatively, at the $2p_{1/2}$ → LUMO resonance, Coster–Kronig Auger decay may also take place, comprising the refill of the Co $2p_{1/2}$ core hole by a $2p_{3/2}$ electron. This creates a Co $2p_{3/2}$ core hole, and the released energy is used to emit an (Auger) electron from an occupied Co 3d level. The Co $2p_{3/2}$ core hole is subsequently filled by Co valence electrons from DOMOs or LUMO/LUMO + 3, resulting in the signal detected in the pink and blue shaded areas, respectively. Note that the direct $2p_{3/2}$-level ionization (at the L_2 edge excitation energy) provides another route for emission in this energy range. The high-energy transitions for L_2-edge relaxation are, however, DOMOs and LUMO/LUMO + 3 → $2p_{1/2}$, which lead to the emission intensity in the 785–795 eV range.

Conclusions

PFY-XA measurement (probing valence electron decay) from Co(III) protoporphyrin IX chloride dissolved in DMSO, interpreted with the help of the theoretical DFT/ROCIS calculations, shows that the cobalt centre-ion adopts a low-spin configuration. In addition, the calculations reveal that the cobalt ion is 5-coordinated, binding to four nitrogen atoms and one chloride ion, or 6-coordinated where cobalt binds additionally to an oxygen of the DMSO solvent. The local HOMO–LUMO gap at the Co site was revealed by RIXS measurements with the excitation energy at the pre-absorption edge. We expect that the work presented here will motivate future RIXS studies aimed at exploring the complex electronic-structure interactions of metal-containing biomolecules in the liquid environment.

Acknowledgements

This work was supported by the European Research Council starting grant No. 279344 and Helmholtz-Gemeinschaft *via* the young investigator fund VH-NG-635. K. A. acknowledges the financial support of the Einstein Foundation Berlin for a postdoctoral scholarship.

References

1 L. R. Milgrom, *The Colours of Life: An Introduction to the Chemistry of Porphyrins and Related Compounds*, Oxford University Press, USA, 1997.
2 M. Kotani, *Ann. N. Y. Acad. Sci.*, 1969, **158**, 20–49.
3 J. M. Gottfried, K. Flechtner, A. Kretschmann, T. Lukasczyk and H.-P. Steinrück, *J. Am. Chem. Soc.*, 2006, **128**, 5644–5645.
4 T. E. Shubina, H. Marbach, K. Flechtner, A. Kretschmann, N. Jux, F. Buchner, H.-P. Steinrück, T. Clark and J. M. Gottfried, *J. Am. Chem. Soc.*, 2007, **129**, 9476–9483.
5 M. D. Maines and A. Kappas, *Biochemistry*, 1977, **16**, 419–423.
6 A. Smith, J. Alam, P. V. Escriba and W. T. Morgan, *J. Biol. Chem.*, 1993, **268**, 7365–7371.
7 J. D. Song, S. K. Lee, S. E. Park, K. M. Kim, K. Kim, Y. M. Park and Y. C. Park, *Int. J. Mol. Med.*, 2011, **28**, 841–845.
8 F. Gel'mukhanov and H. Ågren, *Phys. Rep.*, 1999, **312**, 87–330.
9 J. Nordgren and J.-E. Rubensson, *J. Electron Spectrosc. Relat. Phenom.*, 2013, **188**, 3–9.
10 A. J. Achkar, T. Z. Regier, H. Wadati, Y.-J. Kim, H. Zhang and D. G. Hawthorn, *Phys. Rev. B: Condens. Matter Mater. Phys.*, 2011, **83**, 081106.
11 S. Thürmer, R. Seidel, W. Eberhardt, S. E. Bradforth and B. Winter, *J. Am. Chem. Soc.*, 2011, **133**, 12528–12535.
12 R. Seidel, S. Ghadimi, K. M. Lange, S. Bonhommeau, M. A. Soldatov, R. Golnak, A. Kothe, R. Könnecke, A. Soldatov, S. Thürmer, B. Winter and E. F. Aziz, *J. Am. Chem. Soc.*, 2011, **134**, 1600–1605.
13 F. Neese, *Wiley Interdiscip. Rev.: Comput. Mol. Sci.*, 2012, **2**, 73–78.
14 M. Roemelt, D. Maganas, S. DeBeer and F. Neese, *J. Chem. Phys.*, 2013, **138**, 204101.
15 K. Atak, R. Golnak, J. Xiao, E. Suljoti, M. Pflüger, T. Brandenburg, B. Winter and E. F. Aziz, *J. Phys. Chem. B*, 2014, **118**, 9938–9943.
16 S. B. Brown, P. Jones and I. R. Lantzke, *Nature*, 1969, **223**, 960–961.
17 G. S. Collier, J. M. Pratt, C. R. De Wet and C. F. Tshabalala, *Biochem. J.*, 1979, **179**, 281–289.
18 M. D. Gotz, M. A. Soldatov, K. M. Lange, N. Engel, R. Golnak, R. Könnecke, K. Atak, W. Eberhardt and E. F. Aziz, *J. Phys. Chem. Lett.*, 2012, 1619–1623.
19 F. Neese, *Wiley Interdiscip. Rev.: Comput. Mol. Sci.*, 2012, **2**, 73–78.
20 A. D. Becke, *Phys. Rev. A: At., Mol., Opt. Phys.*, 1988, **38**, 3098–3100.
21 A. D. Becke, *J. Chem. Phys.*, 1993, **98**, 5648–5652.
22 F. Weigend and R. Ahlrichs, *Phys. Chem. Chem. Phys.*, 2005, **7**, 3297–3305.
23 E. J. Baerends, D. E. Ellis and P. Ros, *Chem. Phys.*, 1973, **2**, 41–51.
24 B. I. Dunlap, J. W. D. Connolly and J. R. Sabin, *J. Chem. Phys.*, 2008, **71**, 3396–3402.
25 O. Vahtras, J. Almlöf and M. W. Feyereisen, *Chem. Phys. Lett.*, 1993, **213**, 514–518.
26 K. Eichkorn, O. Treutler, H. Öhm, M. Häser and R. Ahlrichs, *Chem. Phys. Lett.*, 1995, **240**, 283–290.
27 K. Eichkorn, F. Weigend, O. Treutler and R. Ahlrichs, *Theor. Chem. Acc.*, 1997, **97**, 119–124.
28 F. Weigend, *Phys. Chem. Chem. Phys.*, 2006, **8**, 1057–1065.
29 P. A. Adams, D. A. Baldwin, C. E. Hepner and J. M. Pratt, *Bioinorg. Chem.*, 1978, **9**, 479–494.
30 D. F. V. Lewis, *Guide to Cytochromes: Structure and Function*, CRC Press, 1996.

